Reduction-Responsive Supramolecular Sheets for Selective Regulation of Facultative Anaerobe Agglutination

Dawoon Lee, Longlong Dong, Ye Rim Kim, Jehan Kim, Myongsoo Lee,* and Yongju Kim*

Stimuli-responsive supramolecular materials have promising biological applications because of their ability to rapidly undergo significant structural changes in response to diverse stimuli. Herein, supramolecular sheets assembled via charge-transfer interactions between the pyrene moiety of a D-mannose-containing amphiphile and 7,7,8,8-tetracyanoquinodimethane (TCNQ) are reported. The supramolecular sheets show reduction-responsive behavior, in which their disassembly is triggered by the reduction of TCNQ by sodium sulfide. In an anaerobic environment, the sheet structure remains intact and the exposed D-mannose moieties induce the agglutination of facultative anaerobes, thereby inhibiting bacterial growth. In contrast, in an aerobic environment, the reduction of TCNQ by the hydrogen sulfide generated by facultative anaerobes causes sheet disassembly. This enables continuous bacterial growth, because the collapsed sheets cannot induce agglutination. Thus, this study presents a novel supramolecular material for the selective regulation of facultative anaerobe growth according to the external environment.

1. Introduction

Noncovalent interactions (e.g., hydrogen bonding, electrostatic, $\pi-\pi$, and ion–ion) are reversible and dynamic because they are weaker than covalent interactions. These interactions play important roles in the formation of supramolecular materials[1–3]

D. Lee, Y. R. Kim, Y. Kim
KU-KIST Graduate School of Converging Science and Technology
Korea University
Seoul 02841, Republic of Korea
E-mail: yongjukim@korea.ac.kr
L. Dong, M. Lee
Department of Chemistry, Shanghai Key Laboratory of Molecular Catalysis
and Innovative Materials
Fudan University
Shanghai 200438, China
E-mail: mslee@fudan.edu.cn
J. Kim
Pohang Accelerator Laboratory
Pohang University of Science and Technology (POSTECH)
Pohang, Gyeongbuk 37673, Republic of Korea
Y. Kim
Department of Integrative Energy Engineering
Korea University
Seoul 02841, Republic of Korea

and are involved in essential biological functions both in vitro and in vivo, such as protein folding, enzymatic activity, and material exchange through cell membranes.[4,5] Stimuli-responsive supramolecular materials undergo assembly or disassembly in response to external stimuli, such as temperature, pH, solvent polarity, pressure, and redox reactions, via dynamic noncovalent interactions.[6–9] Among these materials, those that are redox-responsive have promising biological applications such as sensing and delivery of small molecules.[10,11] For example, Xiong et al. developed reduction-responsive supramolecular spherical nanoparticles to effectively deliver doxorubicin and sorafenib.[12] Sun et al. developed photo- and reduction-responsive supramolecular vesicles containing coumarin moieties and disulfide bonds to deliver small-molecule payloads.[13] Zhang et al. developed oxidation-responsive supramolecular nanoparticles assembled via host–guest interactions between β-cyclodextrin-based polycations and a ferrocene-functionalized zinc tetraaminophthalocyanine core for the release and transfection of plasmid DNA.[14] The ability of redox-responsive supramolecular materials to rapidly change their functionality via the transformation of their chemical structures under the action of reductants or oxidants is well suited for the sophisticated fabrication of dynamic materials.

Microorganisms can be classified as aerobes and anaerobes depending on the type of reactions they use to generate energy for growth and life support.[15] Aerobic growth, which requires oxygen as a terminal electron acceptor, is inhibited in the absence of oxygen, whereas anaerobic growth is inhibited by the oxidative stress caused by the presence of oxygen. Facultative anaerobes, such as *Escherichia coli* (*E. coli*) and *Salmonella*, can grow both in the presence and absence of oxygen,[16] making their environment-dependent proliferation difficult to regulate selectively. In addition, the metabolites produced by facultative anaerobes under aerobic condition differ from those produced under anaerobic condition.[17,18] For example, inorganic reductants such as sulfides, which prevent oxidative stress, are generated in an aerobic environment.[19,20] Another factor that can affect the growth of bacteria is the degree of agglutination, which alters their ability to reproduce and spread. Thus, the regulation of agglutination is a potential strategy for functional materials to control the proliferation of bacteria.[21,22]
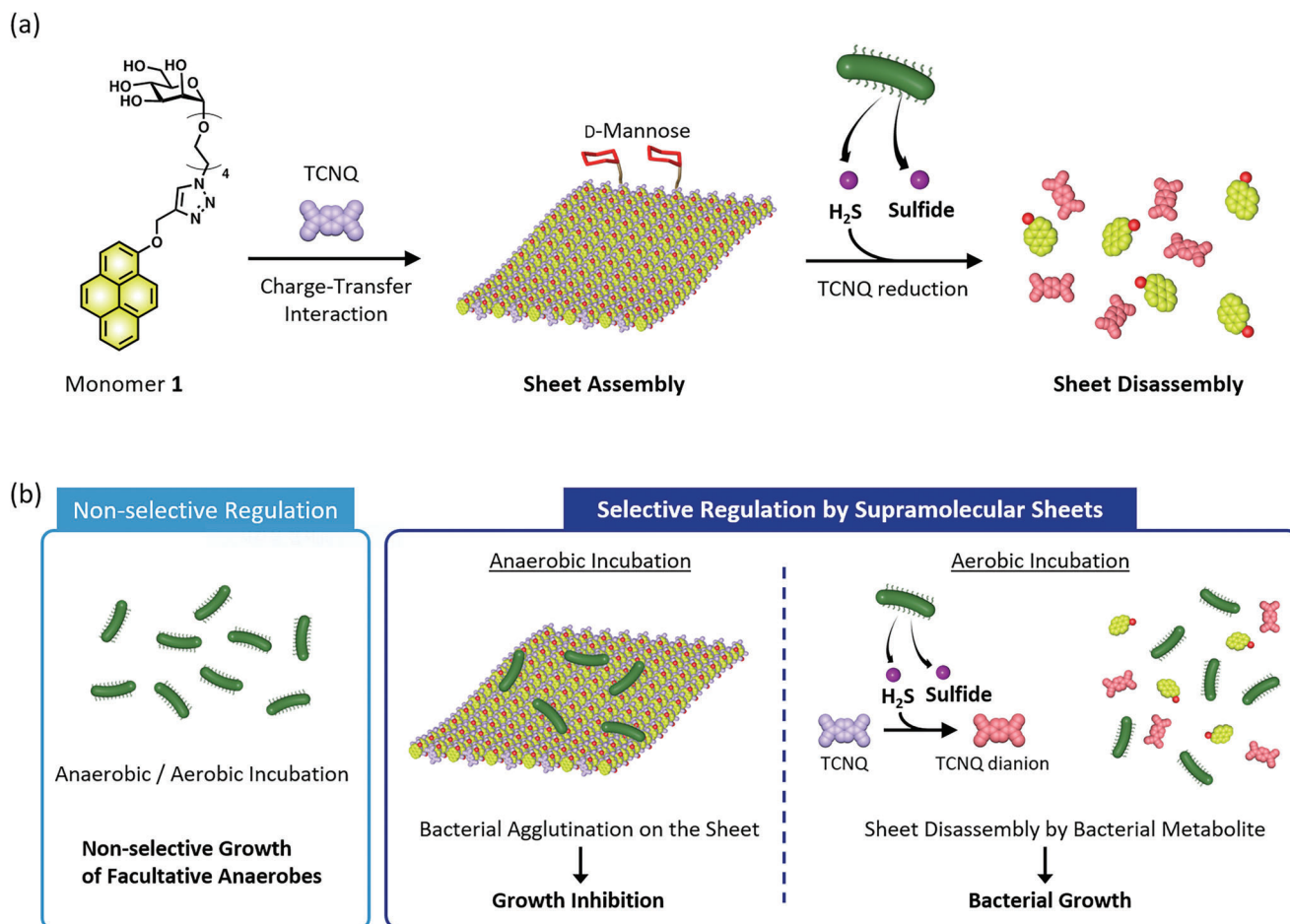
Figure 1. a) Schematic representation of sheet assembly via charge-transfer interactions between **1** and 7,7,8,8-tetracyanoquinodimethane (TCNQ) and sheet disassembly upon hydrogen-sulfide-triggered TCNQ reduction. b) Selective regulation of facultative anaerobe agglutination and growth in anaerobic and aerobic environments by reduction-responsive supramolecular sheets.

Herein, we report reduction-responsive supramolecular sheets that can selectively regulate the agglutination and growth of facultative anaerobes in aerobic and anaerobic environments (**Figure 1**). These supramolecular sheets, which feature surface-exposed D-mannose moieties, are formed by the co-assembly of D-mannose–pyrene-conjugated amphiphile **1** and 7,7,8,8-tetracyanoquinodimethane (TCNQ) via donor–acceptor interactions. The stimulus-responsive behavior of the sheets is provided by the reduction of TCNQ. These reduction-responsive supramolecular sheets have a promising application in cellular-metabolite-triggered selective regulation of biological systems.

2. Results and Discussion

2.1. Structural and Spectroscopic Characterization of the Co-Assembly of 1 with TCNQ

Compound **4** was synthesized by a click reaction between hydrophobic pyrene (**3**) with a terminal acetylene and hydrophilic D-mannose (**2**) with a terminal azide group linked by tetraethylene glycol (Scheme S1, Supporting Information). The

target, amphiphile **1**, was obtained by the deacetylation of the acetyl-protected D-mannose moiety of **4** by sodium methoxide. Amphiphile **1** was characterized by ^{1}H and ^{13}C nuclear magnetic resonance (NMR) spectroscopy (Figures S1 and S2, Supporting Information) and matrix-assisted laser desorption/ionization-time-of-flight mass spectrometry to verify its structure (Figure S3, Supporting Information).

Negative-stain transmission electron microscopy (TEM) analysis of the self-assembly of **1** in an aqueous solution revealed the presence of micelles ≈20 nm in size (Figure S4, Supporting Information), in agreement with the results of dynamic light scattering (DLS) measurements (Figure S5, Supporting Information). Because the pyrene group may engage in donor–acceptor interactions to form a charge-transfer complex, **1** was co-assembled with TCNQ, a π-electron-deficient aromatic molecule, to induce structural changes through enhanced molecular stacking.[23–25] The addition of TCNQ to an aqueous solution of **1** resulted in the emergence of a broad absorption band at 441 nm due to charge-transfer interactions (Figure S6a, Supporting Information) and a change in the solution color from colorless to yellow (Figure S7, Supporting Information).[26] Concomitantly, the fluorescence intensity of the pyrene moiety decreased, and the excimer
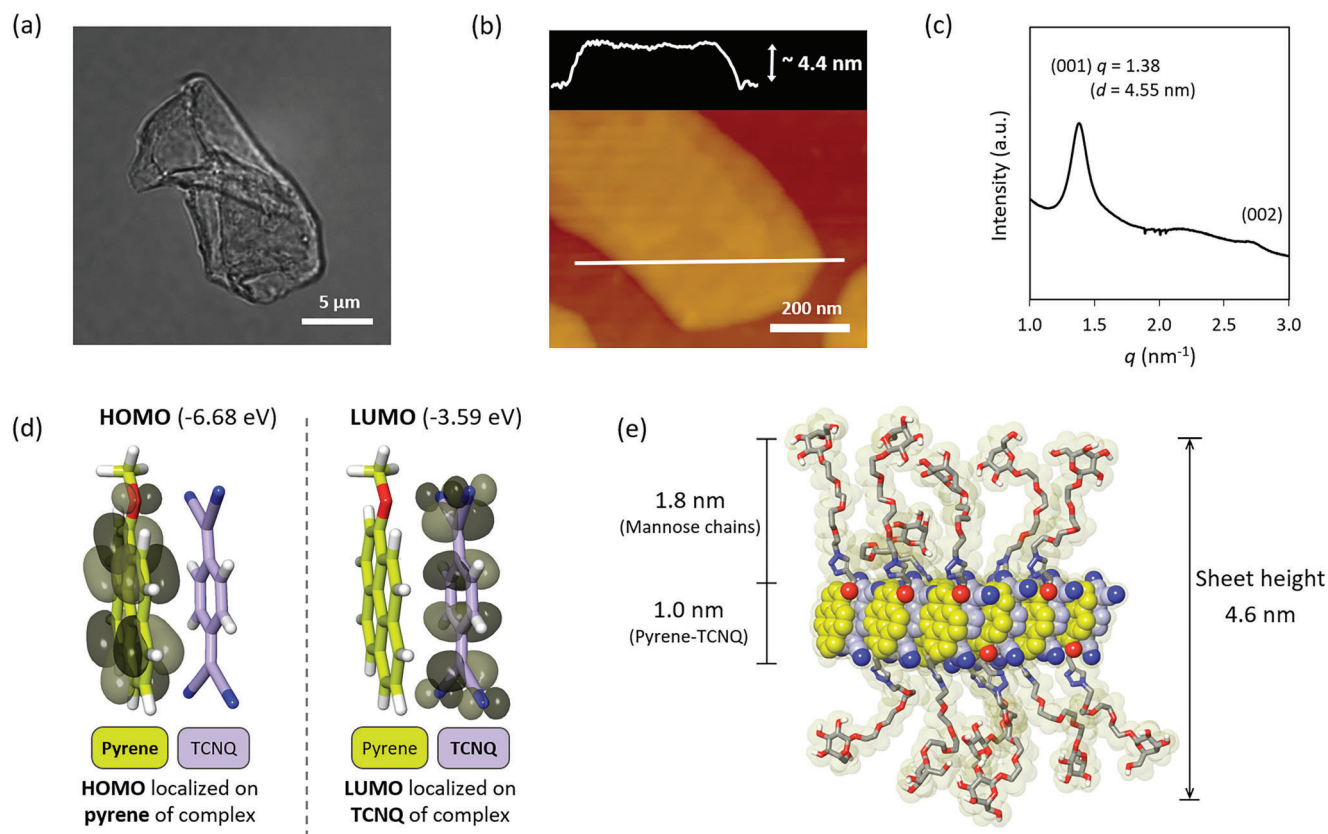
Figure 2. a) Phase-contrast optical microscopy image of **1** (314×10^{-6} M) in an aqueous solution with one equivalent of 7,7,8,8-tetracyanoquinodimethane (TCNQ). b) AFM height profile of the film formed on a mica surface upon the evaporation of a solution of **1** (314×10^{-6} M) with one equivalent of TCNQ. c) SAXS pattern of amphiphile **1** with one equivalent of TCNQ after freeze-drying. d) Frontier molecular orbitals (HOMO: highest occupied molecular orbital; LUMO: lowest unoccupied molecular orbital) of the charge-transfer complex between 1-methoxypyrene and TCNQ calculated by density functional theory. e) Representative image of a supramolecular sheet from molecular dynamics simulations.

peak of pyrene disappeared (Figures S6b and S8, Supporting Information). These results indicate the formation of a charge-transfer complex via the insertion of TCNQ between two stacked pyrene moieties. In addition, in the circular dichroism (CD) spectrum, a signal with a strong Cotton effect was observed in the spectral range of the pyrene segment, confirming the asymmetric intermolecular stacking between pyrene and TCNQ (Figures S6c and S9, Supporting Information).[27] Increasing the amount of TCNQ did not lead to significant changes in all the spectra (Figures S7–S9, Supporting Information), indicating that one equivalent is optimal for co-assembly. Therefore, all further experiments were performed at an amphiphile **1**:TCNQ molar ratio of 1:1.

The structure of the charge-transfer complex was investigated by optical microscopy and negative-stain TEM. Both imaging techniques revealed isolated 2D objects with lateral dimensions of several micrometers, demonstrating the presence of robust, free-standing sheets in the bulk solution (**Figures 2**a and **3**d). In addition, DLS measurements confirmed the formation of a supramolecular assembly several micrometers in size in the presence of TCNQ (Figure S5, Supporting Information). Atomic force microscopy (AFM) analysis of the co-assembly showed the presence of single-layer membranes with a uniform height of ≈4.4 nm (Figure 2b). The small-angle X-ray scattering (SAXS)

pattern revealed a reflection of ≈4.55 nm corresponding to the *d*-spacing between sheets (Figure 2c), which was similar to the thickness obtained by AFM.

The corresponding wide-angle X-ray scattering (WAXS) pattern showed a strong reflection at 3.4 Å associated with the $\pi-\pi$ stacking distance, indicating the close parallel packing of pyrene and TCNQ (Figure S10, Supporting Information). In contrast, the WAXS pattern of **1** in the absence of TCNQ showed a very weak reflection at similar *q* values owing to the lack of crystallinity in the aromatic moieties, indicating weak aromatic interactions. The interaction between pyrene and TCNQ in solution was also investigated by ^{1}H-NMR spectroscopy. The peaks associated with the aromatic protons and OCH_2 moieties of **1** shifted downfield upon the addition of TCNQ, in agreement with the face-centered stacking between pyrene and TCNQ (Figure S11, Supporting Information).[28]

Density functional theory (DFT) calculations further indicated parallel stacking interactions between pyrene and TCNQ. Frontier molecular orbital analysis revealed that the highest occupied molecular orbital (HOMO) and lowest unoccupied molecular orbital (LUMO) are localized on pyrene and TCNQ, respectively. Thus, the transition from the donor (HOMO) to the acceptor (LUMO) is related to charge-transfer complex formation (Figure 2d).[29]
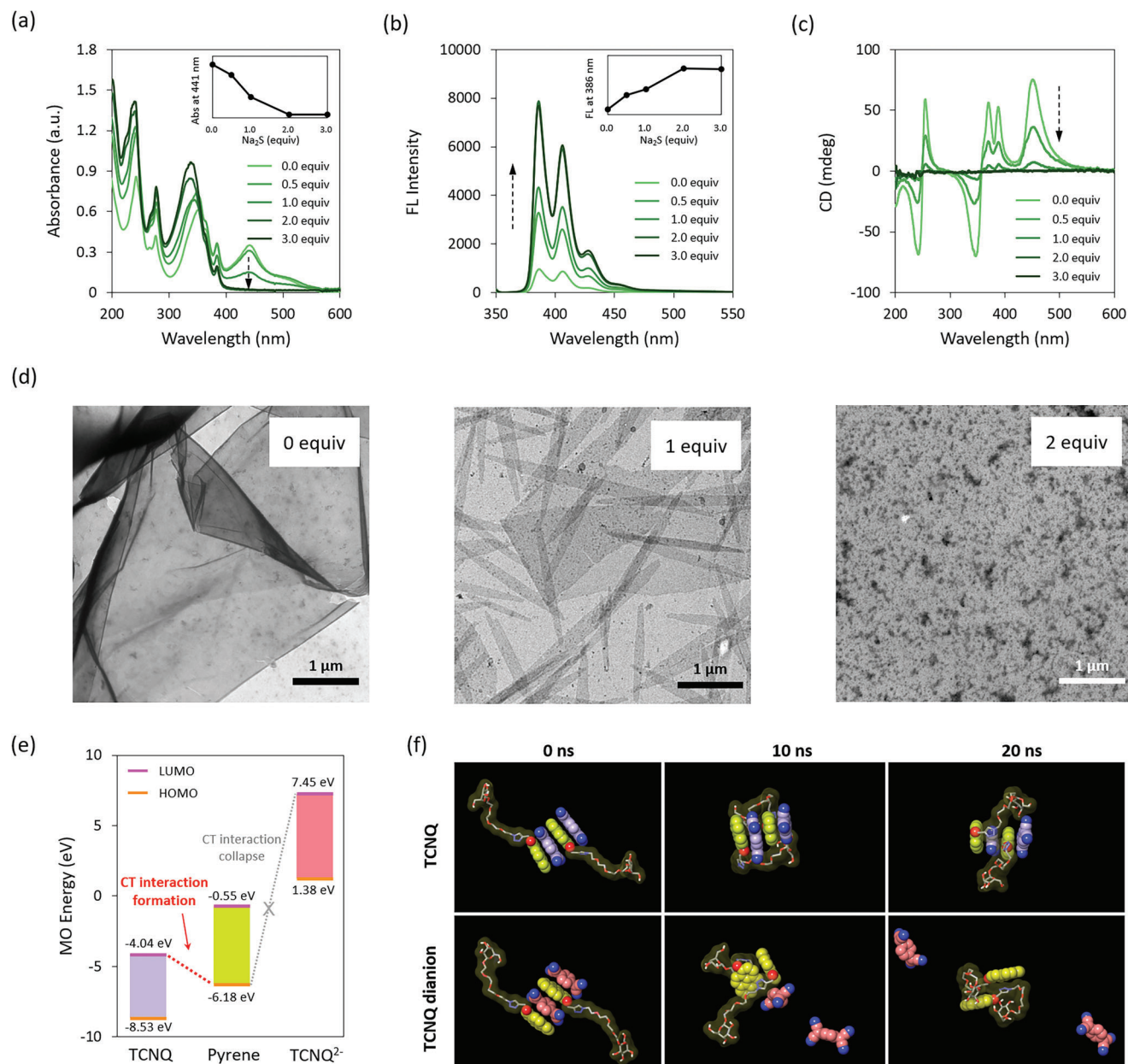
Figure 3. a) Absorption, b) emission (excitation wavelength = 342 nm), and c) CD spectra of the supramolecular sheets treated with different amounts of sodium sulfide. The insets of (a) and (b) show the absorbance at 441 nm and fluorescence (FL) intensity at 386 nm, respectively. d) Negative-stain TEM image of **1** (314×10^{-6} M) with one equivalent of 7,7,8,8-tetracyanoquinodimethane (TCNQ) sequentially treated with different equivalents of sodium sulfide in an aqueous solution. e) Molecular orbital (MO) energy levels of 1-methoxypyrene, TCNQ, and the TCNQ dianion (CT: charge-transfer; HOMO: highest occupied molecular orbital; LUMO: lowest unoccupied molecular orbital). f) Snapshots of the assembly and disassembly of the complexes of **1** with TCNQ and the TCNQ dianion from molecular dynamics simulations (time interval = 10 ns).

Negative-stain TEM was performed at a low concentration (31.4×10^{-6} M) to obtain additional information on sheet formation. As shown in Figure S12 (Supporting Information), the charge-transfer complex consists of laterally associated, individual nanofibers with an average diameter of 4.9 nm. Molecular dynamics (MD) simulations of a sheet composed of 12 amphiphiles showed that the hydrophilic D-mannose units and oligoethylene glycol linkers are exposed on both sides of the hydrophobic pyrene–TCNQ charge-transfer complex (Figure 2e).

Based on the calculated hydrophilic segment length of **1** (1.8 nm) and pyrene height (1.0 nm) (Figure S13, Supporting Information), the height of the sheet estimated by MD simulations is 4.6 nm, which is similar to those obtained by AFM and SAXS.

2.2. Reductant-Induced Disassembly of Supramolecular Sheets

TCNQ, which triggers sheet formation via charge-transfer complexation, can be reduced to anionic products (Figure S14a,

**ADVANCED
SCIENCE NEWS**

www.advancedsciencenews.com

**ADVANCED
HEALTHCARE
MATERIALS**

www.advhealthmat.de

Supporting Information).[30–32] Considering that these products cannot form charge-transfer interactions, we investigated the response of the supramolecular sheets to TCNQ reduction. In a preliminary experiment, TCNQ was reduced using several reducing agents, including sodium sulfide, sodium L-ascorbate, and $NaBH_4$. The corresponding absorption spectra revealed that TCNQ was reduced to a dianion upon treatment with two equivalents of sodium sulfide (Figure S14b, Supporting Information). On the other hand, it was not completely reduced by two equivalents of sodium L-ascorbate (Figure S14c, Supporting Information) but reduced to a monoanion by two equivalents of $NaBH_4$ (Figure S14d, Supporting Information). Thus, sodium sulfide was used as the reductant to investigate the structural changes of the supramolecular sheets upon TCNQ reduction. Addition of sodium sulfide resulted in a decrease in the intensities of the charge-transfer band at 441 nm in the absorption spectrum and signals in the CD spectrum and an increase in the fluorescence intensity of pyrene. No significant changes were observed in all the spectra when more than two equivalents of sodium sulfide were used (Figure 3a–c). In a control experiment, incubation of pure **1** with sodium sulfide did not cause a change in the retention time measured by high-performance liquid chromatography analysis (Figure S15, Supporting Information). These results indicate that the charge-transfer interactions between the pyrene moieties of **1** and TCNQ weakened upon treatment with sodium sulfide because of the reduction of TCNQ. Considering that the sheets were held together by charge-transfer interactions, the spectral changes triggered by TCNQ reduction indicated reduction-responsive behavior.

The structural changes due to sodium sulfide addition were further investigated by negative-stain TEM and scanning electron microscopy (SEM). Notably, the sheets transformed into nanoribbons upon the addition of one equivalent of sodium sulfide and were completely disassembled when two equivalents were added (Figure 3d and Figure S16, Supporting Information). The sheet-to-ribbon transformation suggests the weakening of lateral interactions in the fiber-containing sheets due to the concomitant decrease in the number of charge-transfer interactions.

The molecular orbital energy levels of pyrene, TCNQ, and the TCNQ dianion indicate that sheet disassembly is due to the lack of charge-transfer interaction between pyrene and the TCNQ dianion. In contrast to the bandgap of TCNQ, that of the TCNQ dianion is staggered with respect to the pyrene bandgap, which is indicative of structural collapse (Figure 3e). 20 ns MD simulations of the complexes of **1** with TCNQ and the TCNQ dianion using the simple point-charge (SPC) water model showed the separation of **1** and the TCNQ dianion over time, and at the end of the simulation, only **1** remained assembled by the interaction between the pyrene moieties (Figure 3f). Thus, the supramolecular sheets produced via charge-transfer complexation between pyrene and TCNQ disassembles upon the reduction of TCNQ by sodium sulfide.

2.3. Selective Regulation of Facultative Anaerobe Agglutination and Growth in Different External Environments

D-Mannose, which is a C-2 epimer of D-glucose, is commonly found in nature[33] and has several important roles, such as specific binding to FimH, an adhesive subunit of type-1 fimbriae expressed in almost all bacteria.[34–36] Inspired by this selective binding capability, many researchers used D-mannose to prevent infection by pathogenic bacteria and regulate bacterial proliferation.[22,37,38] In this study, the supramolecular sheets were co-incubated with *E. coli* ORN 178, which expresses FimH in its wild-type pili. TEM, SEM, and fluorescence microscopy images showed agglutinated bacteria on the supramolecular sheets, which noticeably increased in size owing to the interaction between D-mannose and FimH (Figure S17, Supporting Information). In contrast, the supramolecular sheets could not induce the agglutination of *E. coli* ORN 208, which expresses abnormal-type pili that have no FimH that can bind to D-mannose (Figure S18, Supporting Information). These results indicate that the supramolecular sheets induce the agglutination of ORN 178 via specific binding between FimH and D-mannose on the sheet surface.

E. coli is a facultative anaerobe that produces hydrogen sulfide, an inorganic reductant, in an aerobic environment to prevent oxidative stress.[39–41] To investigate hydrogen sulfide production by *E. coli* under aerobic condition, we performed sulfide indole motility experiments. A black color was observed in the bacterial culture medium, indicating hydrogen sulfide production (Figure S19, Supporting Information).[42,43] Inspired by the differential production of hydrogen sulfide by *E. coli* in aerobic and anaerobic environments, we investigated the regulation of *E. coli* proliferation in these environments by the reduction-responsive supramolecular sheets. The bacterial growth of ORN 178 was measured in terms of optical density, which is widely used to estimate the density of cells in liquid media.[44] Bacterial growth was also confirmed by WST-8 assay, which provides colorimetric detection of microbial metabolism (Figure S20, Supporting Information).[45] The growth rate decreased upon the addition of the supramolecular sheets in an anaerobic environment (**Figure 4**a), indicating that the sheet-induced agglutination of ORN 178 inhibits bacterial growth.[21,22,46] In contrast, the growth rate of ORN 178 was maintained in an aerobic environment (Figure 4b). Thus, the effect of supramolecular sheets on bacterial growth depends on the external environment (Figures S21 and S22, Supporting Information).

The CD spectra of the supramolecular sheets incubated with ORN 178 in aerobic and anaerobic environments were measured. In an anaerobic environment, the intensity of the CD signal decreased gradually, and ≈56% of its initial value was retained after 2 h of incubation at 30 °C (Figure 4c,e). As a control experiment, the charge-transfer complex was incubated without bacteria at the same temperature. The CD signal of the charge-transfer complex also decreased gradually, indicating entropically weakened charge-transfer interactions resulting from the increased dynamicity of the hydrophilic segments at higher temperatures (Figure S23, Supporting Information). In contrast, in an aerobic environment, the CD signal rapidly decreased in intensity and disappeared after 2 h of incubation (Figure 4d,e). These results suggest that the metabolites produced by *E. coli* in aerobic and anaerobic environments affect the supramolecular sheet structure differently.

Microscopic imaging of the supramolecular sheets incubated with ORN 178 showed that bacterial agglutination occurred in an anaerobic environment, whereas the supramolecular sheets
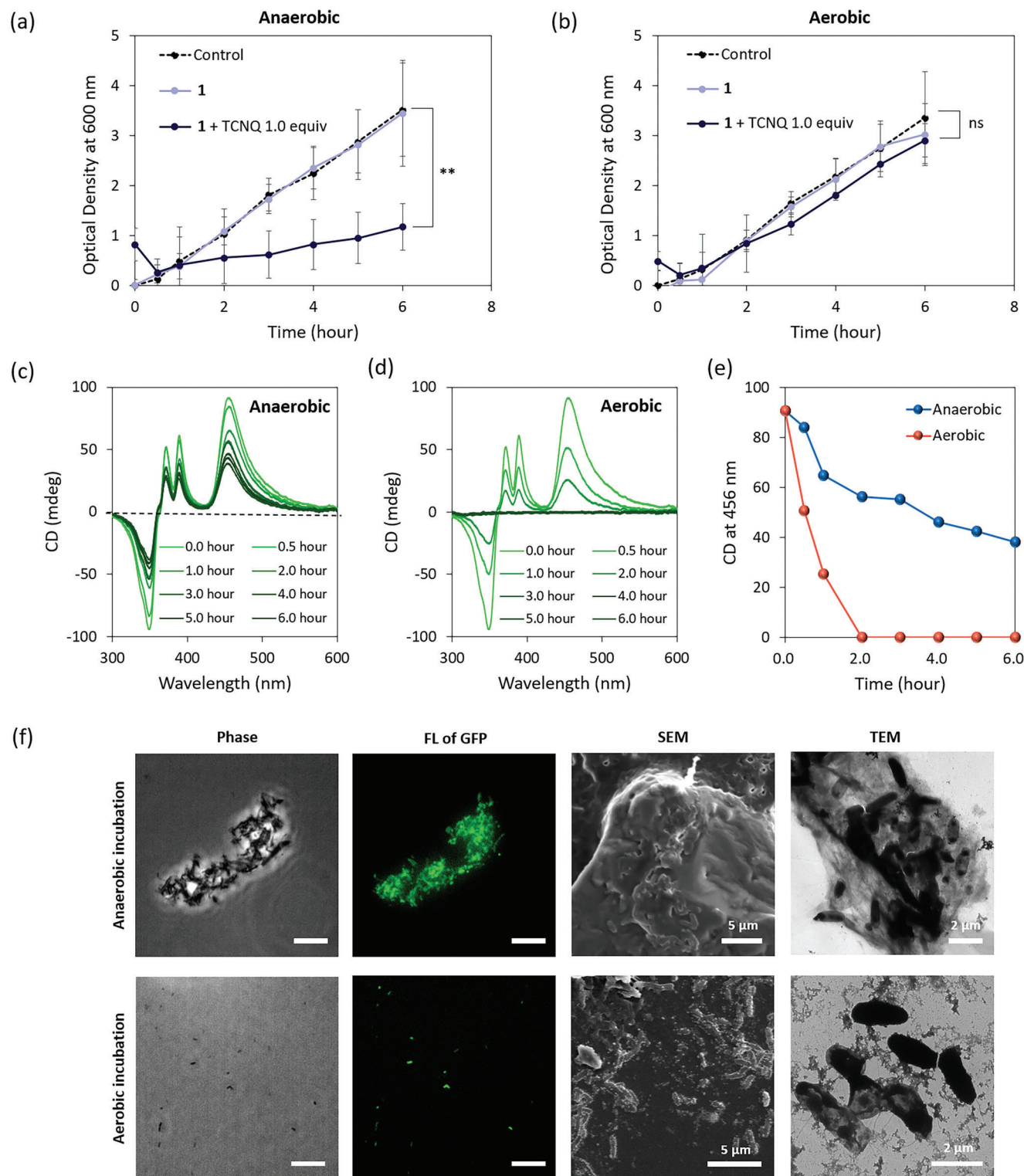
**ADVANCED
SCIENCE NEWS**

www.advancedsciencenews.com

**ADVANCED
HEALTHCARE
MATERIALS**

www.advhealthmat.de

Figure 4. Bacterial growth curves of ORN 178 with **1** (314×10^{-6} M) treated and untreated with 7,7,8,8-tetracyanoquinodimethane (TCNQ) in a) anaerobic and b) aerobic environments. CD spectra of **1** (314×10^{-6} M) treated with one equivalent of TCNQ and exposed to ORN 178 in c) anaerobic and d) aerobic environments. e) Plots of the CD intensity at 456 nm of the supramolecular sheets incubated with ORN 178 in anaerobic and aerobic environments. f) Phase-contrast optical microscopy, fluorescence (FL) microscopy, SEM, and TEM images of the green fluorescence protein (GFP) of ORN 178 after a 2-h incubation with reduction-responsive supramolecular sheets in anaerobic and aerobic environments. Green fluorescence is due to the GFP of ORN 178. The scale bar of the phase-contrast optical microscopy images is 20 μm. **$p < 0.01$ ($n = 5$).

ADVANCED
SCIENCE NEWS

www.advancedsciencenews.com

ADVANCED
HEALTHCARE
MATERIALS

www.advhealthmat.de

collapsed without inducing bacterial agglutination in an aerobic environment (Figure 4f; and Figures S24 and S25, Supporting Information). Thus, the proliferation of *E. coli* in aerobic (growth) and anaerobic (inhibition) environments is controlled by the response of the supramolecular sheets to hydrogen sulfide, a reducing metabolite.

3. Conclusion

Supramolecular sheets with surface-exposed D-mannose moieties were constructed via charge-transfer interactions between the pyrene-based amphiphile **1** and TCNQ. These supramolecular sheets consisted of laterally associated nanofibers in the parallel-stacked charge-transfer complexes and showed reduction-responsive behavior, in which they were disassembled upon the reduction of TCNQ by sodium sulfide. In an anaerobic environment, the exposed D-mannose moieties caused the agglutination of facultative anaerobes by specifically binding to FimH. Consequently, the growth of bacteria was inhibited because of their ability to sense and respond to population density and environmental change. In contrast, in an aerobic environment, facultative anaerobes produced a metabolite, hydrogen sulfide, that induced the collapse of the reduction-responsive supramolecular sheets, resulting in non-agglutination and continuous bacterial growth. The developed supramolecular approach has promising applications in cellular-metabolite-triggered control of biological systems and regulation of the spread of bacterial infections.

4. Experimental Section

Commercial suppliers (TCI and Aldrich, etc.) provided materials, organic reagents, and solvents used in experiments unless otherwise specified. Anhydrous dichloromethane (DCM) was distilled from CaH_2. Deionized water (DW) was prepared via ion exchange and filtration. Thin-layer chromatography (TLC) was conducted in silica gel-coated glass plates (silica gel 60 F254 0.25 nm). The components on TLC plates were visualized under ultraviolet light (254 and 365 nm) or by staining with anisaldehyde, iodine, phosphomolybdic acid, $KMnO_4$, and vanillin. The products were purified using flash column chromatography on silica gel (230–400 mesh). Mass spectrometry was performed by CMS (Advion) Expression mass spectrometer. Analytic and preparatory high-performance liquid chromatography (HPLC) were conducted using LC-20AR (Shimadzu) with YMC-Pack Pro C18 column (250 × 4.6 mm I.D.) and YMC-Actus Triart C18 (250 × 20.0 mm I.D.), respectively. ^{1}H and ^{13}C NMR spectra were obtained by 400 MHz FT-NMR spectrometer, JNM-ECZ400S/L1. The absorption spectra were obtained by Agilent 8453E UV–visible spectrophotometer, and the emission spectra were measured by the Hitachi F-7000 fluorescence spectrophotometer. Using a JASCO J-1100 spectropolarimeter, CD spectra were obtained. DLS at a fixed angle of $\theta = 90°$ was performed to characterize the sizes of the supramolecular structures by using an Otsuka Electronics ELSZ-1000. A transmission mode X-ray scattering measurement was performed at Pohang Accelerator Laboratory using synchrotron radiation.

TEM Experiments: 2–4 µL of the sample solution were drop-casted onto a carbon-coated grid (Carbon Type B on 200 mesh with Formvar; Ted Pella, Inc.). A drop of uranyl acetate aqueous solution (0.4 wt%) was deposited on the sample-loaded grid after evaporating at ambient conditions. The dried specimen was observed by a Hitachi H-7100, and H-7650 operated at 100 kV.

SEM Experiments: The microscope slides were cleaned via traditional piranha solution. 20 µL of sample solution was placed on a piece of microscope slides (25 × 75 mm, ≈1 mm, Heinz Herenz Hamburg) by drop-

casting, and the sample solution was dried under ambient conditions. The sample-loaded microscope slides were coated with Pt (≈4 nm) by Hitachi ion sputter E-1010 and observed by Hitachi S-4300 at 5 kV and 10 µA conditions.

AFM Experiments: 20 µL of sample solutions were drop-casted on mica or SI wafer and evaporated in ambient conditions. The measurements were conducted with an NX-10 (Park systems), and the images were acquired in tapping mode.

Molecular Simulations: Analysis of amphiphile **1** and TCNQ co-assembled sheet structure and disassembly via reduced TCNQ were performed by MacroModel module in Schrödinger Suites (Schrödinger K.K.) with the following parameters; force field: OPLS4, solvent: water, cutoff: none. The energy levels of pyrene, TCNQ, and TCNQ dianion and frontier orbital interaction between pyrene and TCNQ were optimized using the DFT M06-2X (6-31G*) method using Gaussian 09 software. The molecular dynamics simulations for the assembly and disassembly of complexes of **1** with TCNQ and TCNQ dianion were performed via the Desmond module in Schrödinger Suites with the following parameters-force field: OPLS4; solvent model: SPC; boundary conditions: orthorhombic box shape, box size calculation method (buffer); simulation time: 20 ns; approximate number of frames: 100; ensemble class: *NPT*; temperature: 300 K; pressure: 1.01325 bar; thermostat method: Nose–Hoover chain; coulombic interaction cutoff radius: 9.0 Å.

Sampling Methods: TCNQ in CH_3CN and amphiphile **1** in MeOH were mixed, and then the solvents were evaporated under low pressure. For each concentration, deionized water was added to the dried mixture. After that, the aqueous solution was sonicated in a cold bath for 60 min.

Binding to Bacteria of Supramolecular Structures: The bacterial strains ORN 178 GFP and ORN 208 were grown overnight in LB media using ampicillin and tetracycline as selective antibiotics. Following resuspend in the PBS solution, centrifugation was used to collect ORN 178 and ORN 208. The bacteria were added to supramolecules (314×10^{-6} M) in PBS solution. The adhesion and agglutination of bacteria to the sheets were observed using SEM, TEM, and FOM after fixation with a 4% formaldehyde solution. FOM images were measured using the following filter: excitation wavelength 460–500 nm and emission wavelength 520–560 nm.

Bacterial Growth Curve Measurements: The OD_{600} was measured with LB media and diluted to OD_{600} of 1.1–1.2. The optical density measurements depending on time were recorded on a DEN-600 Photometer. This solution (300 µL) was added to each co-assembled amphiphile **1** (314×10^{-6} M), and all samples were put into the incubator at 30 °C with mild shaking in the dark to prevent sedimentation. At each time point, the OD_{600} of each sample was measured. The bacterial growth of ORN 178 was also measured by WST-8 assay (Sigma-Aldrich, Cell Counting Kit-8, CCK-8). CCK-8 solution (10 µL) and the bacterial suspension (190 µL/well) were added to a 96-well plate. After incubating for 1 h, the absorbance at 450 nm was measured.

Statistical Analysis: All tests were repeated three times, and the results were presented as mean ± standard deviation (SD). Student's *t*-test and one-way analysis of variances (ANOVAs) with post-hoc Tukey's honestly significant difference (HSD) comparison test were conducted for statistical comparisons between groups. Statistics are considered significant when nominal p-values are less than 0.05 (Prism-GraphPad, San Diego, CA).

Supporting Information

Supporting Information is available from the Wiley Online Library or from the author.

Acknowledgements

Conflict of Interest

The authors declare no conflict of interest.

Author Contributions

D.L. and L.D. synthesized molecules and performed most of the experiments. Y.R.K. carried out the bacterial viability experiments. J.K. performed X-ray experiments. M.L. and Y.K. developed the concept, supervised the research, and revised the manuscript.

Data Availability Statement

The data that support the findings of this study are available from the corresponding author upon reasonable request.

[1] L. Brunsveld, B. J. B. Folmer, E. W. Meijer, R. P. Sijbesma, *Chem. Rev.* **2001**, *101*, 4071.
[2] T. Aida, E. W. Meijer, S. I. Stupp, *Science* **2012**, *335*, 813.
[3] T. F. A. De Greef, M. M. J. Smulders, M. Wolffs, A. P. H. J. Schenning, R. P. Sijbesma, E. W. Meijer, *Chem. Rev.* **2009**, *109*, 5687.
[4] D. A. Uhlenheuer, K. Petkau, L. Brunsveld, *Chem. Soc. Rev.* **2010**, *39*, 2817.
[5] X. Yan, F. Wang, B. Zheng, F. Huang, *Chem. Soc. Rev.* **2012**, *41*, 6042.
[6] M. Vázquez-González, I. Willner, *Angew. Chem., Int. Ed.* **2020**, *59*, 15342.
[7] H. Shigemitsu, I. Hamachi, *Acc. Chem. Res.* **2017**, *50*, 740.
[8] P. M. Mendes, *Chem. Soc. Rev.* **2008**, *37*, 2512.
[9] Z. Li, N. Song, Y.-W. Yang, *Matter* **2019**, *1*, 345.
[10] D. Li, R. Zhang, G. Liu, Y. Kang, J. Wu, *Adv. Healthcare Mater.* **2020**, *9*, 2000605.
[11] Y. Yuan, T. Nie, Y. Fang, X. You, H. Huang, J. Wu, *J. Mater. Chem. B* **2022**, *10*, 2077.
[12] Q. Xiong, M. Cui, G. Yu, J. Wang, T. Song, *Front. Pharmacol.* **2018**, *9*, 61.
[13] Z. Sun, G. Liu, J. Hu, S. Liu, *Biomacromolecules* **2018**, *19*, 2071.
[14] N. Zhang, Y. Wang, R. Wu, C. Xu, J.-J. Nie, N. Zhao, B. Yu, Z. Liu, F.-J. Xu, *Small* **2019**, *15*, 1904017.
[15] K. H. Schleifer, *Syst. Appl. Microbio.l* **2009**, *32*, 533.
[16] S. T. Rutherford, B. L. Bassler, *Perspect. Med.* **2012**, *2*, a012427.
[17] S. Bury-Moné, N. O. Kaakoush, C. Asencio, F. Mégraud, M. Thibonnier, H. D. Reuse, G. L. Mendz, *Helicobacter* **2006**, *11*, 296.
[18] N. R. Krieg, P. S. Hoffman, *Annu. Rev. Microbiol.* **1986**, *40*, 107.
[19] M. Stieglmeier, R. Wirth, G. Kminek, C. Moissl-Eichinger, *Appl. Environ. Microbiol.* **2009**, *75*, 3484.
[20] T. A. Pankratov, L. A. Kirsanova, E. N. Kaparullina, V. V. Kevbrin, S. N. Dedysh, *Int. J. Syst. Evol. Microbiol.* **2012**, *62*, 430.
[21] J. J. C. Martín, M. Assali, E. Fernández-García, V. Valdivia, E. M. Sánchez-Fernández, J. M. Garcia Fernández, R. E. Wellinger, I. Fernándezc, N. Khiar, *J. Mater. Chem. B* **2016**, *4*, 2028.
[22] D.-W. Lee, T. Kim, I.-S. Park, Z. Huang, M. Lee, *J. Am. Chem. Soc.* **2012**, *134*, 14722.
[23] B. Shen, I.-S. Park, Y. Kim, H. Wang, M. Lee, *Giant* **2021**, *5*, 100045.
[24] R. Usman, A. Khan, H. Sun, M. Wang, *J. Solid State Chem.* **2018**, *266*, 112.
[25] L. Dong, D. Lee, Y. Kim, M. Lee, *J. Polym. Sci.* **2023**, https://onlinelibrary.wiley.com/doi/abs/10.1002/pol.20220745.
[26] Y. Sun, Y. Lei, L. Liao, W. Hu, *Angew. Chem., Int. Ed.* **2017**, *56*, 10352.
[27] M. Liu, L. Zhang, T. Wang, *Chem. Rev.* **2015**, *115*, 7304.
[28] M. Rudloff, K. Ackermann, M. Huth, H. O. Jeschke, M. Tomic, R. Valentí, B. Wolfram, M. Bröring, M. Bolte, D. Chercka, M. Baumgarten, K. Müllen, *Phys. Chem. Chem. Phys.* **2015**, *17*, 4118.
[29] P. Hu, K. Du, F. Wei, H. Jiang, C. Kloc, *Cryst. Growth Des.* **2016**, *16*, 3019.
[30] A. M. Bond, S. Fletcher, F. Marken, S. J. Shaw, P. G. Symons, *J. Chem. Soc., Faraday Trans.* **1996**, *92*, 3925.
[31] G. N. Kamau, J. F. Rusling, *J. Electroanal. Chem. Interfacial Electrochem.* **1990**, *292*, 187.
[32] H. Chang, B. Yi, R. Ma, X. Zhang, H. Zhao, Y. Xi, *Sci. Rep.* **2016**, *6*, 22312.
[33] X. Hu, Y. Shi, P. Zhang, M. Miao, T. Zhang, B. Jiang, *Compr. Rev. Food Sci. Food Saf.* **2016**, *15*, 773.
[34] S. G. Stahlhut, V. Tchesnokova, C. Struve, S. J. Weissman, S. Chattopadhyay, O. Yakovenko, P. Aprikian, E. V. Sokurenko, K. A. Krogfelt, *J. Bacteriol.* **2009**, *191*, 6592.
[35] D. R. Hickling, V. W. Nitti, *Rev. Urol.* **2013**, *15*, 41.
[36] C. H. Jones, J. S. Pinkner, R. Roth, J. Heuser, A. V. Nicholes, S. N. Abraham, S. J. Hultgren, *Proc. Natl. Acad. Sci. USA* **1995**, *92*, 2081.
[37] D. Scribano, M. Sarshar, C. Prezioso, M. Lucarelli, A. Angeloni, C. Zagaglia, A. T. Palamara, C. Ambrosi, *Molecules* **2020**, *25*, 316.
[38] G. Na, Y. He, Y. Kim, M. Lee, *Soft Matter* **2016**, *12*, 2846.
[39] K. Li, Y. Xin, G. Xuan, R. Zhao, H. Liu, Y. Xia, L. Xun, *Front. Microbiol.* **2019**, *10*, 298.
[40] S. Chen, Z.-J. Chen, W. Ren, H.-W. Ai, *J. Am. Chem. Soc.* **2012**, *134*, 9589.
[41] C. E. Cooper, G. C. Brown, *J. Bioenerg. Biomembr.* **2008**, *40*, 533.
[42] P. L. McDonough, S. J. Shin, D. H. Lein, *J. Clin. Microbiol.* **2000**, *38*, 1221.
[43] Y. A. Warren, D. M. Citron, C. V. Merriam, E. J. C. Goldstein, *J. Clin. Microbiol.* **2005**, *43*, 4041.
[44] J. Beal, N. G. Farny, T. Haddock-Angelli, V. Selvarajah, G. S. Baldwin, R. Buckley-Taylor, M. Gershater, D. Kiga, J. Marken, V. Sanchania, C. T. Workman, *Commun. Biol.* **2020**, *3*, 512.
[45] T. Tsukatani, H. Suenaga, T. Higuchi, T. Akao, M. Ishiyama, T. Ezoe, K. Matsumoto, *J. Microbiol. Methods* **2008**, *75*, 109.
[46] N. Krishnan, D. Perumal, S. Atchimnaidu, K. S. Harikrishnan, M. Golla, N. M. Kumar, J. Kalathil, J. Krishna, D. K. Vijayan, R. Varghese, *Chem. - Eur. J.* **2020**, *26*, 1037.